PROCEEDINGS OF THE ROYAL SOCIETY A

rspa.royalsocietypublishing.org

Research

Cite this article: Artoni M, La Rocca GC, Ferrari G. 2014 Quasi-periodic Wannier–Stark ladders from driven atomic Bloch oscillations. *Proc. R. Soc. A* **470**: 20140421.
http://dx.doi.org/10.1098/rspa.2014.0421

Received: 30 May 2014
Accepted: 12 August 2014

Subject Areas:
atomic and molecular physics, mathematical physics, quantum physics

Keywords:
atomic Bloch oscillations, self-similar structures, ultracold atoms

Author for correspondence:
M. Artoni
e-mail: artoni@lens.unifi.it

Royal Society Publishing

Quasi-periodic Wannier–Stark ladders from driven atomic Bloch oscillations

M. Artoni[1,2], G. C. La Rocca[3] and G. Ferrari[2,4]

[1]Department of Engineering and Information Technology, Brescia University, Brescia, Italy
[2]European Laboratory for Nonlinear Spectroscopy (LENS) and Istituto Nazionale di Ottica (INO), Firenze, Italy
[3]Scuola Normale Superiore and CNISM, Pisa, Italy
[4]INO-CNR BEC Center and Dipartimento di Fisica, Trento University, 38123 Povo, Italy

GF, 0000-0003-1827-5048

Periodic Wannier–Stark ladder structures of the energy resonances associated with Bloch oscillations can be readily modified into quasi-periodic ones that exhibit peculiar self-similar effects. A compact theoretical description of the dynamics of driven Bloch oscillations is developed here within the quasi-momentum representation. We identify a rather viable scheme based on ultracold atomic wavepackets subject to gravity in a driven optical lattice potential where a self-similar scaling could be observed. Its feasibility in terms of realistic experimental parameters is also discussed.

1. Introduction

The issue of electrons moving in periodic crystal lattices attracted much attention in the past. Yet, with the advent of optical lattices for ultracold atoms (see [1, 2] and references therein), this issue has gained a renewed interest. Optical lattices, in fact, are increasingly employed for realizing laboratory models of solid crystals, of which Mott-insulator transitions [3], Bloch [4, 5] and super Bloch oscillations [6] are perhaps the most significant examples. More generally, the intrinsic flexibility of optical lattices made from a standing wave of light makes them quite amenable to the study of quantum transport of matter waves and their nonlinear dynamics [1,7].

A quantum particle moving in a periodic potential is characterized by an energy and quasi-momentum lying on well-defined bands and, owing to the potential

translational symmetry, particle wavepackets propagate typically unbound through the potential. When an additional *constant* force is applied, however, the periodic symmetry of the lattice potential is broken, suppressing atomic tunnelling between lattice sites. In this case, the wavepacket can exhibit bound oscillatory motion, performing familiar periodic Bloch oscillations. Following an early suggestion by Esaki & Tsu [8] (see also [9]), electronic Bloch oscillations were first observed in semiconductor superlattices [10–12]. Bloch oscillations of atoms driven by a constant force were then observed [4] in optical lattices and several improvements have followed since, with experiments on thermal samples [13,14], on weakly interacting [5,15,16] and non-interacting condensates [17,18] as well as on non-interacting quantum degenerate fermions [19]. The constant external force is, in this case, created by accelerating the optical lattice, a scheme which has also been employed to observe Rabi oscillations between Bloch bands [20], integer Wannier–Stark ladder resonances [21] and resonantly enhanced tunnelling of Bose–Einstein condensates [22]. When the additional external force is instead *oscillating* in time, the atomic motion in the periodic potential is in general no longer bound, except for special cases and only within the nearest-neighbour tight-binding approximation [23].

In this paper, we study the dynamics of Bloch atoms subjected to a generic time-dependent force, specifically investigating the atoms' dynamics when both a *constant* and an *oscillating* driving force are present. The resulting dynamics is interpreted in terms of Wannier–Stark resonances whose structure is found to depend essentially on how the Bloch oscillation period and the driving period compare with one another. For specific driving configurations, *quasi-periodic* Wannier–Stark ladder structures may arise that exhibit a singular self-similar scaling effect occurring in both the topology and amplitudes of the wavepacket quasi-energy resonances.

We start by providing a compact framework for the description of the dynamics of Bloch atoms subjected to a generic time-dependent force, restricting ourselves, for simplicity, to a single-band and a one-dimensional model, i.e. neglecting Zener tunnelling between bands and hence also decay and disregarding complex optical potential geometries. We similarly neglect nonlinear effects due to atom–atom interactions [14,17–19] here. This gives a tighter focus to the basic mechanism underlying the rather involved dynamics of a Bloch wavepacket subjected to a generic time-dependent driving force. We work in the quasi-momentum representation [24,25], which offers clear advantages when compared with other approaches [26–31]. This is used in §2 to obtain an exact expression for the atom's wave function. A number of exact analytical results for the atom's momentum and position are then derived in §3 for the specific situation in which the force comprises both a constant and an oscillating component. These results are derived both within and beyond the nearest-neighbour coupling approximation and provide a valuable insight into how the purely periodic dynamics induced by either the constant or the oscillating force term may combine to yield periodic as well as non-periodic evolutions. The analytical expressions for position and momentum derived in §3 are particularly amenable to a straightforward interpretation in terms of integer, fractional and quasi-periodic Wannier–Stark ladder resonances and this is done in §4.

It is worth mentioning here that, in spite of a number of theoretical predictions [27–29,32] brought forward over the past decade or so, not much experimental work on the spectroscopy of atomic Wannier–Stark ladders has been carried out [7]. This has mainly focused on the observation of periodic, namely integer [21] and fractional [17,33], Wannier–Stark spectra. Observations of quasi-periodic Wannier–Stark ladders in atomic systems remain elusive. To this end, we present a simple experimental procedure through which quasi-periodic atomic Wannier–Stark ladders and the novel self-similar scaling effects we anticipate may be measured with ultracold atoms in optical lattices. Such self-similar structures may in fact be retrieved with a good experimental resolution, an issue that we address at the end of §4.

2. The model

The atom dynamics in a periodic potential is examined here by referring to an optical potential, i.e. a one-dimensional sinusoidal lattice generated by a standing wave of laser light. Spontaneous

emission can be neglected provided the laser is detuned sufficiently far from the atomic resonance, in which case the effective potential experienced by the atom in its ground state is given by $V(x) = V_o \cos^2(\pi x/a)$. The periodicity a is half the laser light wavelength λ and the amplitude V_o is proportional to the laser intensity and inversely proportional to its detuning from the atom's resonance. When the potential is accelerated through an external time-varying modulation $x_e(t)$ of the standing-wave position, the potential $V_o \cos(\pi x/a - \pi x_e(t)/a)^2$ becomes time-dependent and so is the Hamiltonian in the laboratory frame. The case of a modulation of the form $x_e(t) = x_o + f_o t^2/2m$, for example, can be attained by shifting in frequency the two counter-propagating components of the standing wave by an amount $\Delta\nu = t \times f_o/2\,ma$, increasing linearly with time. The lattice potential is no longer stationary in the *laboratory* frame, yet in the potential *rest* frame where the Hamiltonian is now time-independent the atom experiences a constant inertial force $-f_o$ in addition to the periodic potential $V(x) = V_o \cos^2(\pi x/a)$. The same form of $x_e(t)$ with $f_o/m = g$ is used to assess the effect of the acceleration due to gravity g on the dynamics of atoms in a periodic potential.

For a generic modulation $x_e(t)$, however, the Hamiltonian remains in general time-dependent both in the laboratory and in the optical lattice rest frame. In a one-dimensional periodic potential experiencing a generic acceleration $\ddot{x}_e(t)$, the quantum-mechanical motion of an atom of mass m in the lattice rest frame may be described as being due to the external force $f_e(t) = -m\ddot{x}_e(t)$, which contributes with a linear term in x to the relevant Schrödinger equation

$$i\hbar \frac{\partial \Psi(x,t)}{\partial t} = H_o(x)\Psi(x,t) - x f_e(t)\Psi(x,t). \tag{2.1}$$

The properties of the eigenstates and eigenenergies of the Hamiltonian

$$H_o(x) = \frac{p^2}{2m} + V(x) \tag{2.2}$$

are usually derived from the Bloch theorem stating that the eigenenergies $E_n(k)$ and the eigenstates $\psi_n(k,x)$ of (2.2) are labelled by a discrete band index n and a continuous quasi-momentum k. The eigenfunctions can be written as $\psi_n(k,x) = u_n(k,x)\,e^{ikx}$, where $u_n(k,x)$ is spatially periodic with the same periodicity of the lattice and where $E_n(k)$ are periodic in k with period $2\pi/a$ and the quasi-momentum k is then conventionally reduced to the first Brillouin zone. If the atom's wave function is expressed as a sum over all bands

$$\Psi(x,t) = \sum_{n=1}^{\infty} \int_{-\pi/a}^{\pi/a} dk \phi_n(k,t)\psi_n(k,x) \tag{2.3}$$

we obtain after inserting (2.3) into (2.1) and using the orthogonality properties of the Bloch wave functions

$$i\hbar \frac{\partial \phi_n(k,t)}{\partial t} = E_n(k)\phi_n(k,t) - i f_e(t)\partial_k \phi_n(k,t) - f_e(t) \sum_{n'} Z_{n,n'}(k)\phi_{n'}(k,t) \tag{2.4}$$

with

$$Z_{n,n'}(k) = \frac{2\pi i}{a} \int_{-a/2}^{a/2} dx u_n^*(k,x)\partial_k u_{n'}(k,x), \tag{2.5}$$

where ∂_k denotes the derivative with respect to k. This is the Schrödinger equation for the atom's wave function $\phi_n(k,t)$ in the quasi-momentum representation. The terms in (2.5) comprise intraband ($n = n'$) as well as interband ($n \neq n'$) couplings caused by the external force $f_e(t)$. If all interband couplings are neglected the sum on the right-hand side of (2.4) reduces to the diagonal term $Z_{n,n}(k)$. Restricting ourselves *only* to the single nth band the diagonal matrix element $Z_{n,n}(k)$ can be further set to vanish.[1] In the following, all terms in (2.5) are neglected.

[1]For symmetric potentials $V(x) = V(-x)$ and a suitable choice of the phase of the Bloch eigenfunctions, i.e. $\psi_n(k,-x) = \psi_n^*(k,x)$, the diagonal matrix elements $Z_{n,n}(k)$ in (2.5), can be taken to be zero (e.g. [34]).

By using the method of characteristics [35] and with the help of the transformation

$$t=\tau \quad k=q+\frac{1}{\hbar}\int_0^\tau \mathrm{d}\tau' f_e(\tau')\equiv q+\theta(\tau), \tag{2.6}$$

where $\theta(\tau)$ represents the atom's instantaneous quasi-momentum displacement, the partial differential equation (2.4) can be reduced to the first-order (ordinary) differential equation

$$\mathrm{i}\hbar\partial_\tau\phi_n(q,\tau)=E_n(q+\theta(\tau))\phi_n(q,\tau), \tag{2.7}$$

whose integration with constant q yields

$$\phi_n(q,\tau)=\phi_n(q,0)\exp\left[-\frac{\mathrm{i}}{\hbar}\int_0^\tau \mathrm{d}\tau' E_n(q+\theta(\tau'))\right]. \tag{2.8}$$

Upon restoring the original variables k and t explicit solutions of (2.4) can be rewritten as

$$\phi_n(k,t)=\phi_n(k-\theta(t),0)\exp\left[-\frac{\mathrm{i}}{\hbar}\int_0^t \mathrm{d}t' E_n(k-\theta(t)+\theta(t'))\right]. \tag{2.9}$$

The first factor on the right-hand side of (2.9) stands for the initial wave function $\phi_n(k,0)$ with k being replaced by $k-\theta(t)$. The relevant atom's wave function finally becomes[2]

$$\Psi(x,t)=\int_{-\pi/a}^{\pi/a}\mathrm{d}k\,\phi(k-\theta(t),0)\psi(k,x)\exp\left[-\frac{\mathrm{i}}{\hbar}\int_0^t \mathrm{d}t' E(k+\theta(t')-\theta(t))\right], \tag{2.10}$$

where the band index n will hereafter be omitted since only atomic states formed from Bloch eigenstates in a single band are considered.

3. The atom quasi-momentum, momentum and position

The mean quasi-momentum can be directly evaluated from (2.10) to yield

$$\langle k(t)\rangle=\int_{-\pi/a}^{\pi/a}\mathrm{d}k\,k|\phi(k-\theta(t),0)|^2, \tag{3.1}$$

whose evolution clearly relies on the form of the quasi-momentum displacement $\theta(t)$. This is particularly apparent for a static force f_o and a narrow initial distribution $\phi(k,0)$ centred at k_o, in which case (3.1) yields $\langle k(t)\rangle\simeq k_o+(f_o/\hbar)t$. The atomic wavepacket moves uniformly through the k space spanning the *reduced* Brillouin zone in a time $T_o=h/(af_o)$ in accordance with what one would expect classically for a particle of momentum $\hbar k$. When the wavepacket approaches the zone boundaries, however, an umklapp process will take place, i.e. the atom's wavevector will change by a reciprocal lattice vector and will appear at the opposite point of the reduced Brillouin zone and the process will repeat itself.

The atom's momentum expectation value, defined as

$$\langle p(t)\rangle=-\mathrm{i}\hbar\int_{-\infty}^{+\infty}\mathrm{d}x\,\Psi^*(x,t)\partial_x\Psi(x,t), \tag{3.2}$$

hinges instead on the evaluation of the Bloch states' momentum matrix elements. These can be shown to be

$$-\mathrm{i}\int_{-\infty}^{+\infty}\mathrm{d}x\psi^*(k',x)\partial_x\psi(k,x)=\delta(k-k')\frac{\partial_k E(k)}{\hbar^2/m}, \tag{3.3}$$

leading to a mean momentum

$$\langle p(t)\rangle=\frac{m}{\hbar}\int_{-\pi/a}^{\pi/a}\mathrm{d}k|\phi(k-\theta(t),0)|^2\partial_k E(k), \tag{3.4}$$

correctly expressed as a superposition of k components having group velocity $\partial_k E(k)/\hbar$ and weighted by the corresponding probability density acquired by the atom at time t.

[2]The atom's wave function $\Psi(x,t)$ remains at all times normalized to unity, i.e. $\int_{-\pi/a}^{\pi/a}\mathrm{d}k|\phi(k-\theta(t))|^2=1$.

The atom's position expectation value, on the other hand, can be derived directly from (2.1), which can be rewritten as

$$f_e(t)\langle x(t)\rangle = \int_{-\infty}^{+\infty} dx \Psi^*(x,t)[H_o(x) - i\hbar\partial_t]\Psi(x,t). \tag{3.5}$$

The integral can be performed analytically and full details are given in appendix A, where we obtain the following expression for the mean position:

$$\langle x(t)\rangle = \frac{1}{\hbar}\int_{-\pi/a}^{\pi/a} dk |\phi(k-\theta(t),0)|^2 \partial_k \int_0^t E[k+\theta(t')-\theta(t)]\, dt'. \tag{3.6}$$

Rather than using the *reduced* Brillouin zone scheme above in which umklapp processes take place at the first Brillouin zone boundary, it is worth noting that the quasi-momentum evolution can equivalently be studied by considering a *repeated* Brillouin zone scheme [24]. Owing to the periodicity in k of the band dispersion and provided that $\phi(k-\theta(t))$ remains non-negligible well within a single reciprocal lattice period, the atom wave function may indeed be defined in this case over the entire k space.[3]

(a) The nearest-neighbour tight-binding approximation

Standard laser cooling techniques enable one to tailor at will the initial quasi-momentum distribution of the atom, which will be taken here to be in the form of a *Gaussian* centred at $k_o = 0$, i.e.

$$\phi(k,0) = \frac{1}{(\pi\sigma^2)^{1/4}} e^{-k^2/2\sigma^2}. \tag{3.7}$$

Because atoms with a spread smaller than the photon recoil momentum may easily be prepared, quasi-momentum widths σ much smaller than the Brillouin zone width $2\pi/a$ may be attained.

In this section, we will further restrict our considerations only to *nearest-neighbour* couplings between the lattice sites of the periodic potential $V(x)$ in (2.2). In this case, the energy dispersion for the lowest band takes the form [24]

$$E(k) = -W\cos(ka), \tag{3.8}$$

where $2W$ is the band full-width. From (3.4) and (3.7), we obtain

$$\langle p(t)\rangle = \frac{mWa}{\hbar\sigma\sqrt{\pi}}\int_{-\infty}^{\infty} dk\, e^{-[k-\theta(t)]^2/\sigma^2}\sin(ka), \tag{3.9}$$

where the repeated Brillouin zone discussed in the previous section has been adopted here. The integral in (3.9) can be carried out,

$$\langle p(t)\rangle = \frac{mWa}{\hbar} e^{-a^2\sigma^2/4}\sin\left[\frac{a}{\hbar}\int_0^t dt' f_e(t')\right], \tag{3.10}$$

and for an accelerating external force of the form

$$f_e(t) = f_o + f\cos(\omega t) \tag{3.11}$$

it reduces to

$$\langle p(t)\rangle = \frac{mWa}{\hbar} e^{-a^2\sigma^2/4}\sin\left[\omega_o t\left(1+\frac{f}{f_o}\frac{\sin\omega t}{\omega t}\right)\right], \tag{3.12}$$

where $\omega_o \equiv 2\pi/T_o = af_o/\hbar$.

In the simplest case of a *time-independent* force term f_o, the periodic symmetry of $H_o(x)$ is broken, suppressing atomic tunnelling between lattice sites. Atomic states then become localized,

[3]In the *extended* Brillouin zone scheme, the integrals over k in equations (3.4) and (3.6) extend from $-\infty$ to $+\infty$ and the evolution of $\langle p(t)\rangle/m$ in (3.4) is straightforwardly recovered from $\langle x(t)\rangle$ upon differentiation.

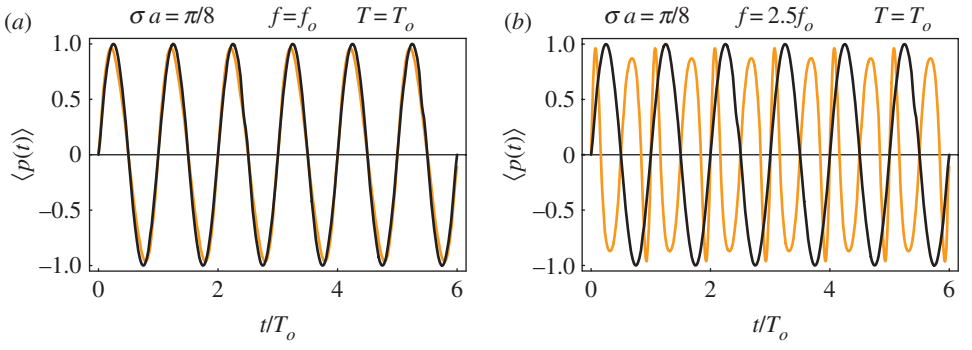

Figure 1. (*a*,*b*) Momentum evolution of an atomic wavepacket of width σ in a periodically driven optical lattice for different driving strengths f and a fixed driving period T. The characteristic Bloch oscillation (3.13) with period T_o for an initial wavepacket of vanishing width and subject only to the constant force f_o is also shown (dark curve) for comparison in both frames. The momentum is in units of $mWa/\hbar$. (Online version in colour.)

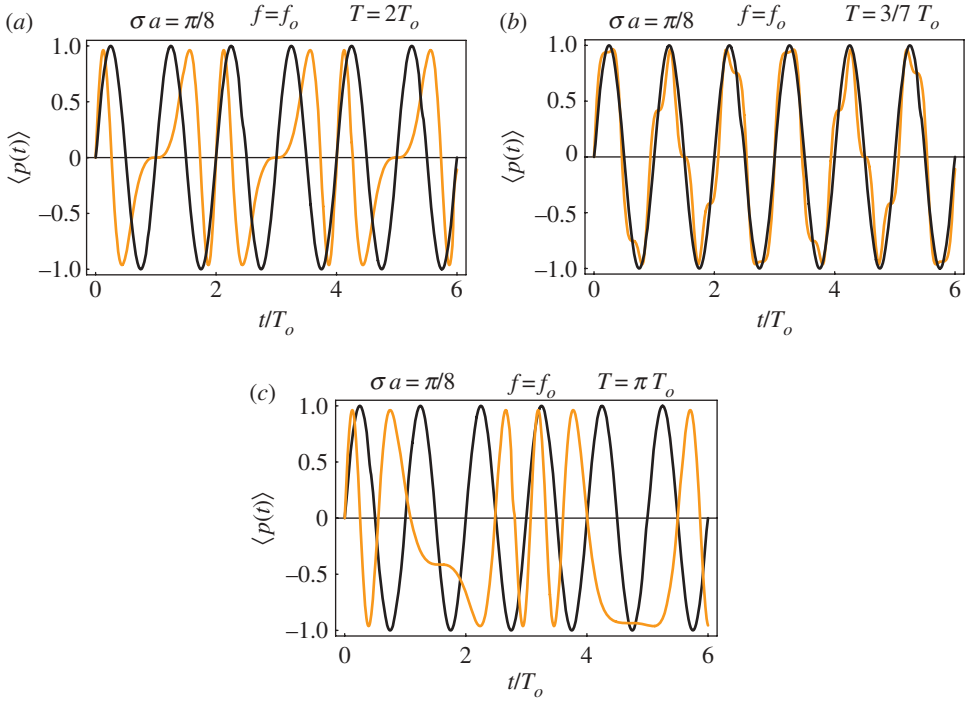

Figure 2. (*a*–*c*) Periodic and non-periodic momentum evolution of an atomic wavepacket of width σ for different driving periods T that are, respectively, commensurate and incommensurate multiples of T_o. The notation is otherwise the same as in figure 1. (Online version in colour.)

giving rise to familiar *Bloch oscillations* at the Bloch frequency ω_o

$$\langle p(t)\rangle = \frac{mWa}{\hbar}\sin(\omega_o t), \tag{3.13}$$

which is obtained from (3.12) in the limit in which $\sigma \to 0$ and $f \to 0$. For *time-dependent* external force $f_e(t)$ in (3.11), however, the driving period T sets an additional time scale and the atom dynamics crucially depends on the relative magnitude of T and T_o as well as on that of f and f_o as shown in figures 1 and 2.

The effect of a time-dependent frequency modulation on the momentum is already clear in figure 1, which shows the momentum for different f/f_o ratios at a fixed modulation period T. The frequency chirp in (3.12) is directly proportional to the ratio f/f_o so that stronger modulation strengths make the atom undergo more complex oscillations, yet maintain in this case the same periodicity. The situation becomes more involved, however, when, for a fixed value of f/f_o as shown in figure 2, the modulation period T is specifically set to acquire *integer*, *rational* and *irrational* multiple values of T_o. Here the momentum is plotted for *rational* values $T/T_o = p/q$ (p, q *integers*), which comprises the limit case of *integer* values $T/T_o = p$, as well as for irrational values of T/T_o. Unlike in the latter case, in which the typical periodicity of the momentum oscillations is lost at least for appreciable strengths f/f_o, in the case of integer and rational values of T/T_o the momentum evolution remains fully periodic.[4] The periodicity is in this case given by pT_o as inferred by inspection of (3.12).

The momenta have been plotted for an initial distribution of non-vanishing widths and compared with the familiar oscillations occurring when only the static term f_o is present (black curve). The broadening only reduces the oscillation amplitudes. To the extent to which only the periodic or non-periodic nature of the evolution is to be examined, broadening may then simply be neglected. It is also worth noting that for a sufficiently narrow initial distribution the exact quantum-mechanical evolution of the momentum in (3.4) correctly recovers the momentum evolution of a classical particle. For a single band, in fact, the particle velocity $(1/\hbar)\partial_k E(k)$ depends on time through its quasi-momentum whose time evolution $k(t) \simeq \theta(t)$, as determined from (3.1) for a narrow distribution, leads to a momentum time-dependence of the form $p(t) \simeq (m/\hbar)\partial_k E(\theta(t))$. When only a constant force f_o is present, for example, $k(t) \simeq f_o t/\hbar$ evolves linearly in time so that the periodicity of the dispersion $E(k)$ directly entails momentum oscillations of the same form [4] and a frequency given by $af_o/\hbar$.

For the same initial distribution (3.7) and energy dispersion (3.8) used in this paragraph, yet for a generic external force $f_e(t)$, the atoms' mean position (3.6) can be rewritten as

$$\begin{aligned}\langle x(t)\rangle &= \frac{W}{\hbar}\int_{-\infty}^{\infty} \mathrm{d}k' \frac{\mathrm{e}^{-k'^2/(a\sigma)^2}}{\sigma\sqrt{\pi}} \int_0^t \sin[k' + a\theta(t')]\,\mathrm{d}t' \\ &= \frac{Wa}{\hbar}\,\mathrm{e}^{-a^2\sigma^2/4}\int_0^t \mathrm{d}t' \sin\left[\frac{a}{\hbar}\int_0^{t'} \mathrm{d}t'' f_e(t'')\right]. \end{aligned} \tag{3.14}$$

As in (3.10) the repeated Brillouin zone scheme has been used while the last expression on the right-hand side of (3.14) can be obtained from a standard Gaussian integration procedure [35]. For the accelerating force (3.11), this reduces to

$$\langle x(t)\rangle = \frac{Wa}{\hbar}\,\mathrm{e}^{-a^2\sigma^2/4}\int_0^t \mathrm{d}t' \sin\left[\omega_o t'\left(1 + \frac{f}{f_o}\frac{\sin\omega t'}{\omega t'}\right)\right] \tag{3.15}$$

or to the familiar Bloch oscillations with amplitude $2W/f_o$

$$\langle x(t)\rangle = \frac{2W}{f_o}\sin^2\left(\frac{\omega_o t}{2}\right), \tag{3.16}$$

when, for a vanishing wavepacket width, the accelerating external force comprises only the constant term (f_o).

(b) Beyond the nearest-neighbour approximation

The tight-binding approximation, by which only neighbouring sites are directly coupled to one another, leads to a rather useful cosine approximation for a band dispersion. In realistic situations, however, more than one neighbour may be coupled to a given lattice site. The resulting dispersion

[4]Floquet theory [30,31] can also be applied to this situation, provided we deal with a periodicity that is not simply the period T associated with the oscillating component of the force, but rather an integer multiple of it and at once also an integer multiple of the Bloch period T_o associated with the constant component (e.g. [27,28]).

may turn out to have a more complicated form. For a given band, the dispersion $E(k)$ may be derived from the eigenvalue equation

$$H_o(x)\psi(k,x) = E(k)\psi(k,x) \tag{3.17}$$

with the help of the orthogonality properties of the Bloch eigenfunctions $\psi(k,x)$. If the matrix elements of $H_o(x)$ are rewritten in terms of localized Wannier functions, departures from the tight-binding approximation may be modelled by taking matrix elements in the form $\langle m|H_o|m'\rangle = -(W/2)\,\mathrm{e}^{-\beta|m-m'|}$. Here again W is related to the width of the band while β^{-1} denotes the range of an exponentially decaying coupling between Wannier states at sites m and m'. After some algebra, we arrive at[5] the dispersion

$$E(k) = \frac{W}{2}\frac{\sinh(\beta)}{\cos(ka) - \cosh(\beta)}, \tag{3.18}$$

which shows increasingly shrinking band-widths for decreasing values of the coupling range β^{-1}.

Upon inserting (3.18) into (3.4) and proceeding as done in (3.9), we obtain

$$\langle p(t)\rangle = \frac{mWa}{\hbar}\frac{\sinh(\beta)}{2}\int_{-\infty}^{\infty} \mathrm{d}k \frac{\mathrm{e}^{-k^2/\sigma^2}}{\sigma\sqrt{\pi}}\frac{\sin(ka - a\theta(t))}{[\cos(ka - a\theta(t)) - \cosh\beta]^2}. \tag{3.19}$$

Since the initial distribution broadening does not affect the evolution (quasi) periodic structure we may simply take here $\sigma \to 0$; the first factor in (3.19) becomes a $\delta(k)$, yielding a momentum

$$\langle p(t)\rangle \simeq \frac{mWa}{\hbar}\frac{\sinh(\beta)}{2}\frac{\sin(a\theta(t))}{[\cos(a\theta(t)) - \cosh\beta]^2} \tag{3.20}$$

whose evolution is determined by a periodic function of the quasi-momentum displacement θ. If the driving (3.11) is used, the argument of these functions takes the same form as that appearing in the square bracket on the right-hand side of (3.12) and this is shown in figure 3 for different values of the coupling range β^{-1} either in the absence or in the presence of external driving. The prominent feature of these oscillations is their asymmetry, which obviously reflects the departure of the actual dispersion from the typical 'cos' relation. Such an asymmetry, which has been observed in experimental measurements of Bloch oscillations of ultracold atoms [4], hinges on the fact that the atom performs a coherent motion over several coupled sites. Similar considerations may be drawn for the atom's mean position and will not be repeated here.

4. The atom quasi-energy spectra: integer, fractional and quasi-periodic cases

It is instructive to Fourier decompose the time evolution of the peculiar atom dynamics observed in §3. Fourier series are commonly used, in fact, to represent the response of a system to a periodic input. We will deal here, for instance, with the atom's momentum by examining both the case of nearest-neighbour interactions and the more general case in which neighbouring sites are coupled to one another. Since broadening affects essentially only the amplitude of the oscillations while leaving the oscillation time evolution unaltered, we will further restrict ourselves to a vanishingly narrow initial distribution specifically referring to the results (3.12), in the appropriate limit in which $\sigma \to 0$, and (3.20).

We start by examining the case $T = (p/q)T_o$, with p and q integers. When the external driving (3.11) is used, $\langle p(t)\rangle$ becomes an odd function of time with period qT as inferred from (3.12). The relevant sine-Fourier decomposition reads as

$$\langle p(t)\rangle = \sum_{r=1}^{\infty} b_r \sin\left(\frac{2\pi}{qT}rt\right) \tag{4.1}$$

with frequency components

$$\omega_r \equiv \frac{2\pi}{qT}r = \frac{\omega_o}{p}r \quad \left(T = \frac{p}{q}T_o\right) \tag{4.2}$$

[5]Similarly, the 'cos' band dispersion (3.8) is easily obtained by taking as matrix elements $\langle 0|H_o|0\rangle = W$ and $\langle 0|H_o|m\rangle = -(W/2)\delta_{m,\pm 1}$.

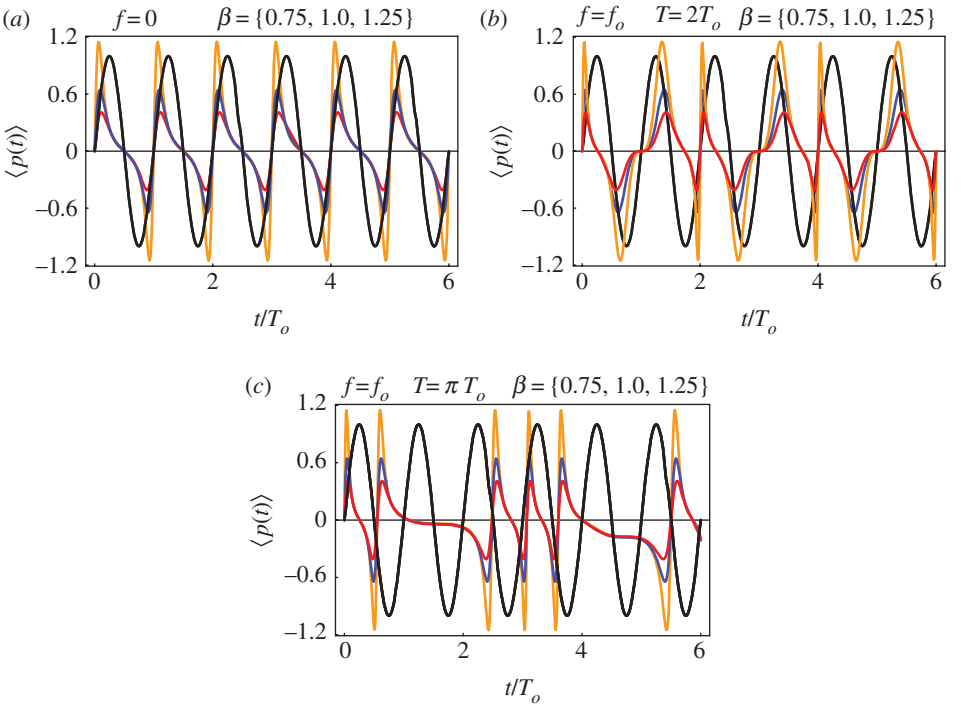

Figure 3. (*a–c*) Momentum evolution of a narrow atomic wavepacket ($\sigma \to 0$) with and without external driving when neighbouring sites coupling with range β^{-1} is taken into account (see §3*b*). The evolution profiles are displayed for the three different values $\beta = 0.75$, $\beta = 1.00$ and $\beta = 1.25$ and have amplitudes that become smaller and smaller with increasing β's. The notation is otherwise the same as in figure 1. (Online version in colour.)

spaced by an integral fraction (ω_o/p) of the Bloch frequency. The corresponding amplitude

$$b_r = \frac{2}{qT}\int_0^{qT} \mathrm{d}t \langle p(t)\rangle \sin\left(\frac{2\pi r}{qT}t\right) \tag{4.3}$$

yields instead the strength with which the different Fourier components contribute to the specific momentum evolution pattern. When, on the other hand, $T = mT_o$, with m integer, $\langle p(t)\rangle$ is an odd function with period T and exhibits an expansion similar to (4.1) with frequencies and amplitudes given, respectively, by

$$\omega_r \equiv \frac{2\pi}{T}r = \frac{\omega_o}{m}r \quad (T = mT_o) \tag{4.4}$$

and

$$b_r = \frac{2}{T}\int_0^{T} \mathrm{d}t \langle p(t)\rangle \sin\left(\frac{2\pi r}{T}t\right). \tag{4.5}$$

The momentum Fourier frequency components turn out to be separated by integer multiples of the ratio ω_o/p or ω_o/m, respectively, suggesting that the evolution of the momentum observed in the previous section may be directly associated with the different modifications that Bloch bands experience under the influence of an external force.

In the presence of a *static* force, a Bloch band splits, in fact, into a series of equally spaced energy resonances separated by *integer* multiples of the Bloch frequency (ω_o). If the force is sufficiently weak Landau–Zener tunnelling between bands can be neglected and the atomic motion becomes periodic, performing oscillations at the characteristic Bloch frequency ω_o.[6] As

[6]For the rather deep optical lattices considered here, say $V_o > 10\hbar^2\pi^2/(2ma^2)$, a conservative estimate leads to $af_o, af < 2\hbar^2\pi^2/(2ma^2)$, following, for example, [28].

anticipated already by Wannier, these oscillations are associated with such an 'integer' Wannier–Stark ladder structure of the *energy* resonances. When the external force also comprises a *time-dependent* driving of period T in addition to the static contribution, the Wannier–Stark ladder modifies into a new one whose separation now depends on how the two periods T and T_o scale with one another and, in particular, on whether the two periods are commensurate or incommensurate.

For *commensurate* ratios, the integer ladder that one has for a static force is replaced by a *fractional* ladder as the relevant quasi-energy resonances are now separated by irreducible fractions of the Bloch frequency ω_o just exactly as they appear in (4.2) and (4.4) for the two specific commensurate values of the ratio T/T_o examined there. The complex periodic oscillations observed in figures 1–3 can then be associated with this 'fractional' Wannier–Stark ladder structure of the *quasi-energy* resonances. For *incommensurate* values of T/T_o, however, $\langle p(t)\rangle$ is no longer periodic in time and a Bloch band does not split into quasi-energy resonances with a fractional ladder structure. This may be seen, for example, directly from (3.12). In the limit $\sigma \to 0$, we have

$$\langle p(t)\rangle = \frac{mWa}{\hbar}\sin(\omega_o t + \alpha \sin \omega t), \quad \left(\alpha \equiv \frac{T}{T_o}\frac{f}{f_o}\right), \tag{4.6}$$

where α is the ratio of the momentum acquired over a cycle of the time-dependent force component to that of the static one. With the help of the Jacobi–Anger expansion (e.g. [35], p. 681), the *sin*-function on the right-hand side of (4.6) may be decomposed to obtain the following momentum expansion:[7]

$$\langle p(t)\rangle = \sum_{r=-\infty}^{\infty} B_r \sin[(\omega_o + r\omega)t], \tag{4.7}$$

with amplitudes[8]

$$B_r = \frac{mWa}{\hbar} J_r(\alpha), \tag{4.8}$$

proportional to the Bessel function $J_r(\alpha)$ of integer order r and frequency components $\omega_r = (\omega_o + r\omega)$. The complex oscillations observed in figure 2*c*, for example, arise then from this peculiar Wannier–Stark ladder structure of the *quasi-energy* resonances, each contributing with a weight (4.8) to the overall momentum evolution.

Furthermore, relaxing the tight-binding approximation and specifically considering exponentially coupled neighbouring sites as in §3*b*, the discussion follows along similar lines. When the external driving comprises both a time-dependent and a static component, a Bloch band splits into several quasi-energy *sub-bands* with a fractional or quasi-periodic Wannier–Stark ladder structure depending on whether the ratio T/T_o acquires as before commensurate or incommensurate values, respectively. We may illustrate this point here by first Fourier decomposing the momentum in (3.20) with respect to $a\theta$. This is an odd function of period 2π and the resulting *sin*-Fourier components turn out to be of the form (4.6), whose decomposition (4.7) may then be used to arrive at the following expansion:

$$\langle p(t)\rangle = \sum_{n=-\infty}^{\infty}\sum_{r=-\infty}^{\infty} B_{n,r} \sin[(r\omega_o + n\omega)t)] \tag{4.9}$$

with amplitudes

$$B_{n,r} = \frac{mWa}{\hbar}\frac{J_n(\alpha r)\sinh\beta}{4\pi}\int_0^{2\pi} \mathrm{d}\xi \frac{\sin\xi \sin(\xi r)}{(\cos\xi - \cosh\beta)^2} \tag{4.10}$$

and frequency components $\omega_{n,r} = (r\omega_o + n\omega)$, which now depend on the two integers n and r. The time evolution described in (4.9) is a typical quasi-periodic one, which is the simplest example of a deterministic, but non-periodic, behaviour.

[7]Note that when T and T_o are commensurate the amplitudes and frequency components in (4.7) (*tight-binding*) recover those obtained from (4.2) to (4.5) and likewise for the amplitudes and frequency components in (4.9) (*beyond tight-binding*).

[8]In spite of an abuse of notation, we differently denote amplitudes associated with commensurate (b_r) or incommensurate (B_r) ratios of T/T_o.

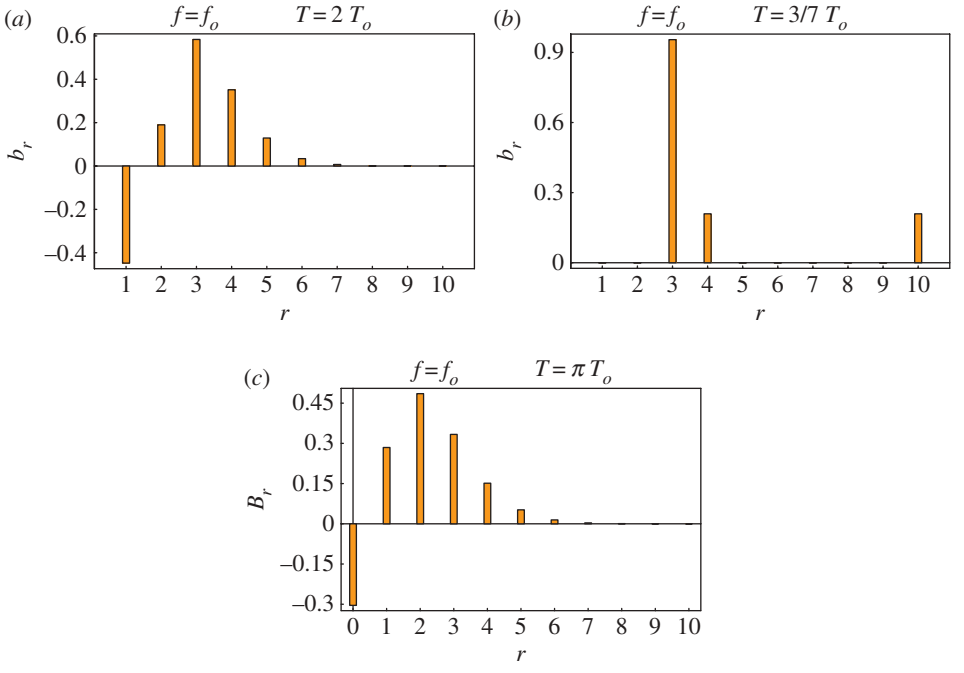

Figure 4. (*a–c*) *Tight-binding approximation*. Momentum Fourier amplitudes b_r in (4.5) and B_r in (4.8) for the three evolution patterns in figure 2. Amplitudes are in units of $mWa/\hbar$. (Online version in colour.)

For *commensurate* ratios T/T_o, the momentum amplitude b's can be evaluated from (4.3) and (4.5). We report in figure 4, for example, the main amplitudes corresponding to the first two evolutions shown in figure 2. While for the rational case ($T/T_o = 3/7$) the dominant contribution is clearly the one at ω_o, that is, when $\omega_3 \to \omega_o$ at $r = 3$, for the integer case ($T/T_o = 2$) a number of appreciable components other than ω_o are instead seen to contribute to the atomic evolution. This is exactly what gives rise to larger departures from the characteristic Bloch oscillations in the case of rational T/T_o ratios of figure 2 (black curve). We report in figure 5*a* the enhancing effect that neighbouring sites coupling has on the Fourier amplitudes. When compared with the corresponding case in figure 4*a*, where only nearest neighbour coupling is considered, appreciable components become available also at large r.

For *incommensurate* ratios T/T_o, the momentum amplitudes B can be evaluated from (4.8) and (4.10). We plot in figure 4*c* the main amplitudes B_r ($r \geq 0$) from (4.8) contributing to the momentum evolution shown in figure 2*c*. The remaining components ($r < 0$) are readily obtained from the relation $B_{-r} = (-)^r B_r$. In figure 5*b*, we report instead the momentum amplitude components for an atomic wavepacket subject to the same driving parameters, yet in the presence of exponentially decaying couplings between neighbouring sites. As in figure 4*c*, the largest contributions occur over the first modes and decrease rather quickly as n and r increase. Again it is sufficient to report here only positive mode amplitude $B_{n,r}(\{n, r\} \geq 0)$.[9]

We report in figure 6*a*, the Fourier transform of (3.20), which shows delta function peaks at each frequency of the form $(r\omega_o + n\omega) \equiv \tilde{\omega}\omega$, as implied by the corresponding decomposition (4.9). The frequency components $\tilde{\omega} = n + r(T/T_o)$ are no longer equally spaced in this case, directly assessing the cross over between the periodic and quasi-periodic quasi-energy structure of driven atoms in optical lattices. For typical quasi-periodic functions, an ever-increasing number of such peaks with smaller and smaller weights densely fill the frequency axis, yet the emerging overall shape of the spectrum is far from being without a structure. It exhibits in fact a recursive [36] pattern

[9]The remaining ones follow directly from the relations $B_{n,-r} = (-)^{n+1} B_{n,r}$, $B_{-n,r} = (-)^n B_{n,r}$ and $B_{-n,-r} = -B_{n,r}$.

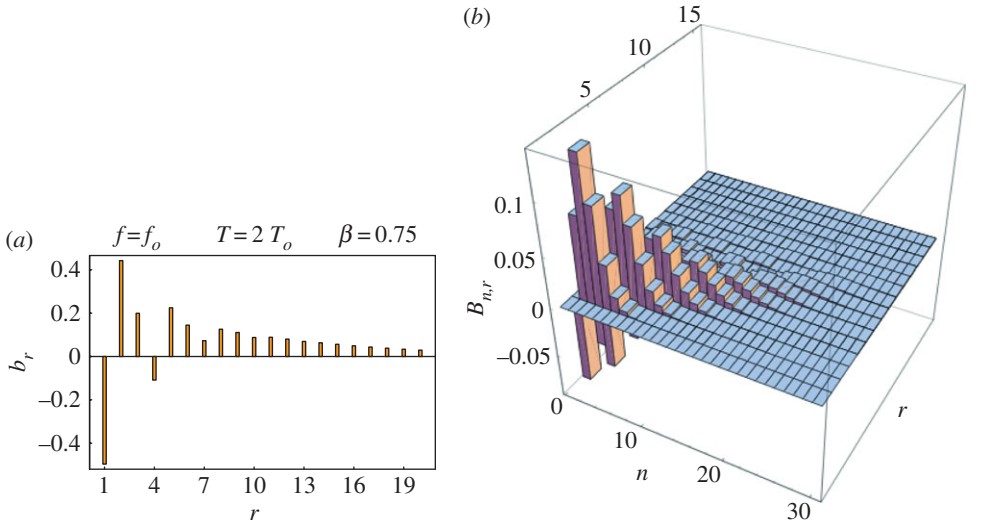

Figure 5. *Beyond tight-binding approximation.* (*a*) Momentum Fourier amplitudes b_r in (4.5) for the evolution pattern in figure 3*b* with $T = 2T_o$. (*b*) Amplitude components $B_{n,r}$ (4.10) for the evolution pattern in figure 3*c* with $T = \pi T_o$. Both amplitudes in units of $mWa/\hbar$ are for the same site-to-site coupling range (β^{-1}) with $\beta = 0.75$. (Online version in colour.)

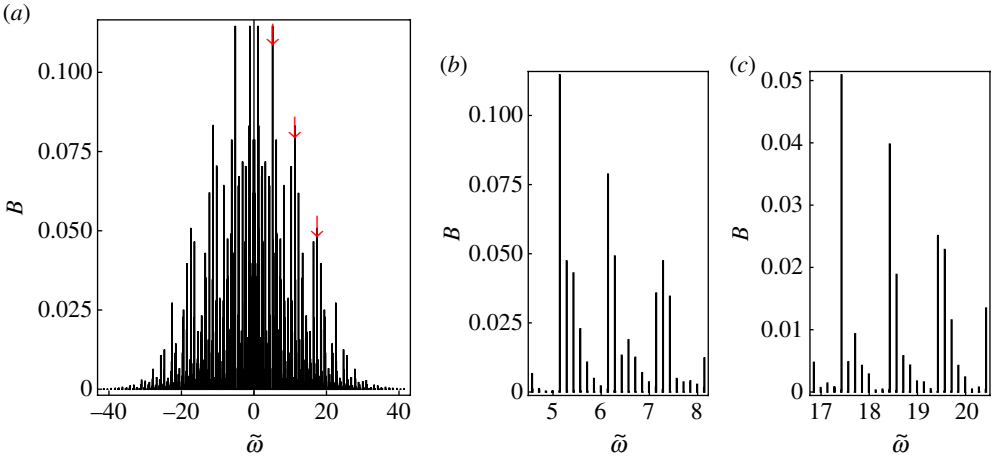

Figure 6. *Beyond tight-binding approximation.* Amplitude components (*a*) for the frequency spectral range corresponding to $-10 \leq (n, r) \leq 10$ in figure 5*b* for the same driving parameters. Spectrum blow-ups (*b*, *c*) showing the characteristic dense filling with weaker and weaker amplitude components. The two blow-up panels (*b*, *c*) represent the spectral regions indicated by the first and third arrow in the whole spectrum (*a*). The similarity of the spectra hints at the self-similarity of a Cantor-like structure. The amplitude components $B_{n,r}$ are suitably relabelled as B while the frequencies components $\omega_{n,r} = (r\omega_o + n\omega)$ are here expressed in units of the driving frequency ω and relabelled as $\tilde{\omega} = n + r\pi$. (Online version in colour.)

characteristic of *self-similar* phenomena and which hinges in our case on the way in which our sub-bands cluster themselves together. As an example, we have marked in figure 6*a* with red arrows a pattern of three prominent peaks in the range $0 \lesssim \tilde{\omega} \lesssim 20$. The same pattern is found again in figure 6*b*,*c*, where the quasi-energy amplitudes are shown over the smaller spectral ranges $5 \lesssim \tilde{\omega} \lesssim 8$ (figure 6*b*) and $17 \lesssim \tilde{\omega} \lesssim 20$ (figure 6*c*), respectively, associated with the first

and the third peaks marked in figure 6*a*. This hints at a definite self-similar scaling of the quasi-energy amplitudes with a hierarchical structure of clusters appearing over smaller and smaller frequency ranges.[10]

Although self-similar features are quite common in deterministic non-periodic systems, the specific system we examine here makes self-similar scaling in the quasi-energy amplitudes of a driven atomic wavepacket in a gravitational field amenable to direct experimental observation. Our ratio T/T_o plays in fact a role similar to that of the Hofstadter scaling parameter in the electronic problem, namely the ratio between the magnetic flux through a lattice cell and the flux quantum [37]. By loading atoms into a vertically aligned optical potential and subject to the gravity force g one implements in fact the static Hamiltonian $H_o(x) + V(x)$ generating, under suitable conditions [14], coherent Bloch oscillations at frequency $\omega_o = mag/\hbar$ that may easily be maintained for seconds. The time-varying external modulation (3.11), which is responsible for the time-periodic-dependent part of the Hamiltonian, is instead realized through a modulation in phase of one of the counter-propagating beams generating the lattice potential [38] or in a retro-reflected configuration with a reflecting mirror mounted on a piezo-electric transducer subject to a driving tension at frequency ω [39]. By recording the atom's momentum evolution at different values of ω and extracting its Fourier components $\tilde{\omega}$, one directly obtains the quasi-energy spectrum of the driven Bloch oscillations. For typical Bloch periods $T_o \simeq 2\,\mathrm{ms}$ and a periodic driving at $T/T_o = \pi$, spectra such as the one in figure 6 could indeed be easily measured either for commensurate or for incommensurate ratios T/T_o through sampling over 1 s at a rate of 10 kHz [14]. This is done in figure 7, where we simulate a typical spectral measurement. The Fourier spectrum calculated from equation (3.19) is sampled during 1 s of the velocity evolution. We also verified that such a spectrum is in quantitative agreement with the spectral weight of the Fourier components in equation (4.10). The three-peak structure shown by the arrows in figure 7*a* may be easily recognized in the other two blow-ups (figure 7*b*,*c*) representing two different regions of the spectrum. In the latter, the fine details are limited by the realistically chosen energy resolution used for the plots. Although, in general, the experimental resolution[11] may limit the observation of a self-similar structure down to finer scales, the realistically broadened spectra reported here already indicate a rather manifest self-similar (pattern) behaviour. We have also checked that the self-similar structure of the spectra is essentially maintained for variations of T/T_0 of the order of a few per cent with only small changes in some of the amplitudes of the frequency components. This is not to say that this novel behaviour of driven atomic wavepackets could easily be unveiled, but such an intriguing spectrum certainly deserves thorough experimental testing.

It is finally worth noting that the above procedure may also be employed to observe self-similar scaling effects in the dynamics of a periodically driven atomic wavepacket directly in the topology of the quasi-energies in the $\{\tilde{\omega}, T/T_o\}$ plane [41]. Pairs of $\{\tilde{\omega}, T/T_o\}$ may indeed be mapped as shown in figure 8 for rational values of T/T_o between 0 and 1. Of course, the reconstruction of the complete spectrum in figure 8 entails a dense ensemble of driving frequencies and hence comes at the expense of a substantial effort in terms of acquisition time. The spectrum discloses in great detail and order the symmetries and subsequent *recursive* topological structure of the atom's quasi-energy. These become particularly conspicuous when quasi-energies are clustered into groups with the characteristic shape of a 'kite'. An extraordinary degree of self-similarity is seen, for example, in figure 8*a*, where upon a suitable resizing of the two scale parameters T/T_o and $\tilde{\omega}$ one obtains four self-similar kite-like patterns that can be fitted into the spectrum skeleton to form an exactly self-similar larger kite pattern (*ABCD*). This spectrum, with a pattern which is symmetric with respect to the origin, repeats itself recursively over $\tilde{\omega}$ regions placed at (integer) multiples of the interval $[0, 1]$ as shown, for example, in figure 8*b*. Owing to a further

[10]Owing to the cut-off values for n and r employed in figure 6, the main $\tilde{\omega}$ spacing appearing in these spectra corresponds to $\pi - 3 \simeq 1/7$, i.e. to $r = 1$ and $n = -3$.

[11]Fourier-limited resolution is also expected in this case as for Hamiltonian systems following a periodic evolution [39].

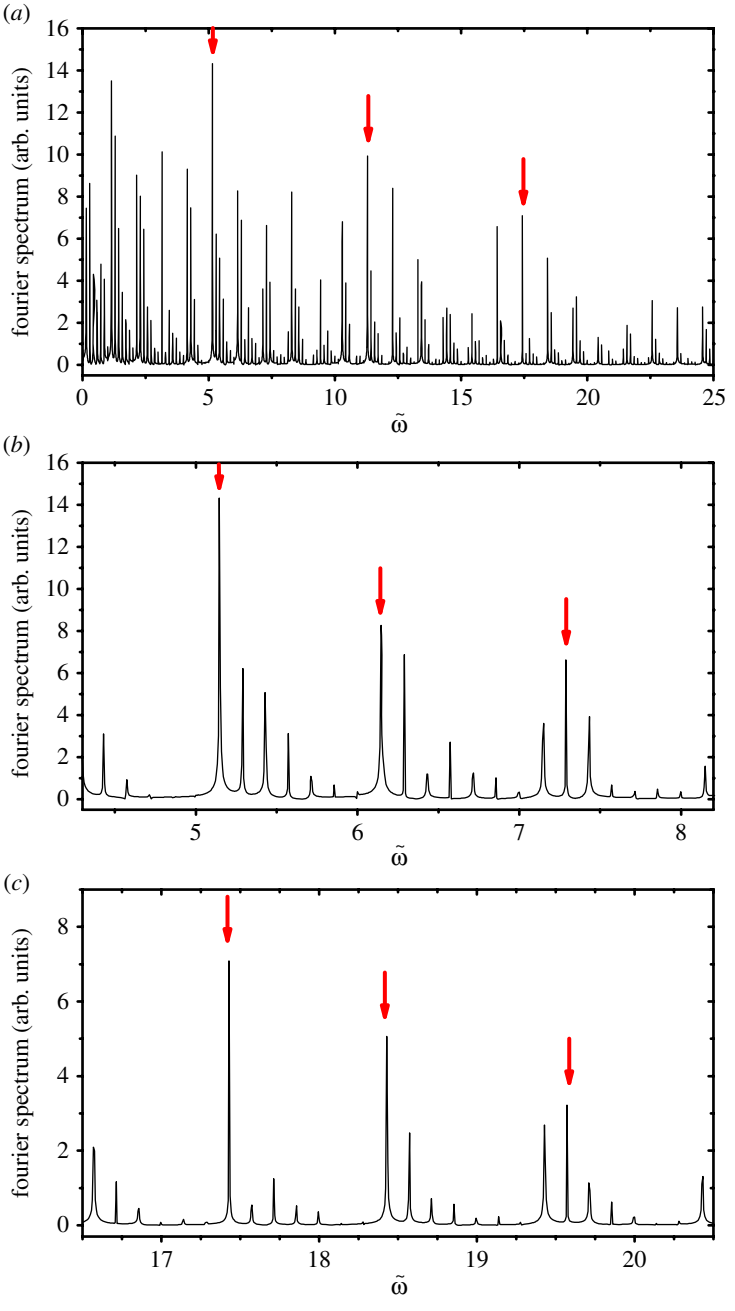

Figure 7. Fourier-simulated spectrum of the atomic velocity for a Bloch period $T_0 = 2$ ms and $T/T_0 = \pi$. The numerically simulated relative weights match those analytically calculated and shown in figure 6. The pattern structure of the complete spectrum (*a*) is recovered in the blow-up sections in panels (*b*) and (*c*) corresponding, respectively, to the spectral regions indicated by the first and third arrow of the upper panel (*a*). The resonance widths are Fourier limited by the integration time set to be 1 s, which corresponds to realistic experimental conditions [39,40]. Frequencies are scaled as in figure 6. (Online version in colour.)

symmetry upon reflection about $T/T_o = 1/2$, the same recursive structure can be observed in the upper part ($AB'CD'$) of the spectrum of figure 8*a* spanning rational values of T/T_o between 1/2 and 1.

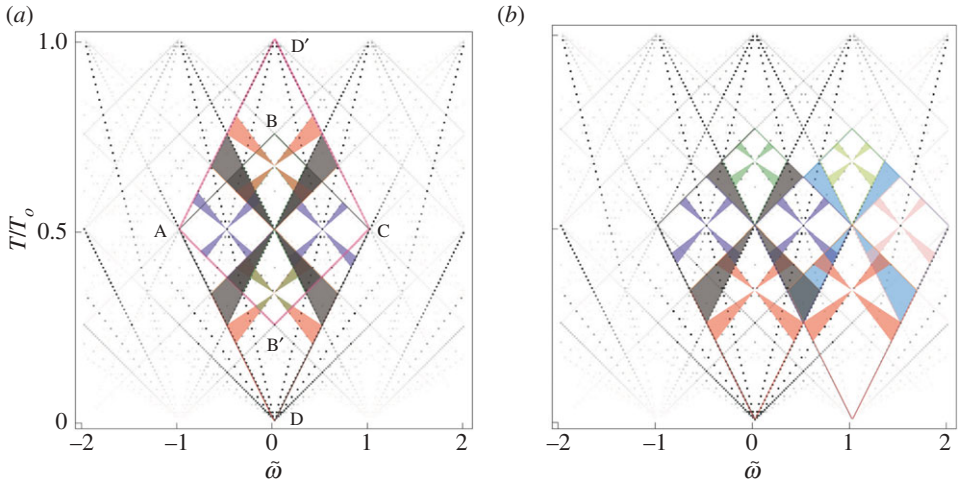

Figure 8. Atomic quasi-energy $\{\tilde{\omega}, T/T_0\}$ spectra. Both spectral component weights, represented here by the dot size,[12] and topology show a characteristic recursive 'kite-like' pattern that can be clearly identified when a colour is associated with each kite cluster. (*a*) Under a suitable resizing of the two scale parameters T/T_0 and $\tilde{\omega}$, one obtains four self-similar kite-like patterns that can be fitted into a spectrum skeleton to form an exactly self-similar larger kite pattern (ABCD). Owing to a further symmetry upon reflection of the pattern about $T/T_0 = 1/2$, the same recursive structure can be observed in the upper part (AB′CD′) of the spectrum. (*b*) The recursive pattern is also symmetric with respect to the origin repeating itself over frequency regions placed at integer multiples of the interval [0,1]. Frequencies are scaled as in figure 6. (Online version in colour.)

5. Conclusion

We study quasi-periodic Wannier–Stark ladder structures that could occur in the evolution of ultracold atomic wavepackets subject to gravity in a driven optical lattice potential. This is done by using realistic experimental parameters for well-resolved and long-lived atomic Bloch oscillations routinely achieved in time-modulated lattices [42,43]. The atom's wavepacket dynamics is studied within a compact framework provided by the quasi-momentum representation. At variance with the fairly involved Floquet theory approach, the explicit form of the wave function in (2.10) provides direct access to all the relevant dynamics, yielding in most cases exact expressions for the wavepacket momentum and position. Besides recovering well-known results associated with Wannier–Stark spectra with periodic ladders of energy resonances, the atom's dynamics studied here is further seen to exhibit peculiar Bloch oscillations relating instead to quasi-periodic Wannier–Stark distributions of quasi-energy resonances. In this quasi-periodic regime, the atom's momentum spectrum exhibits a definite self-similar scaling with a hierarchical structure in both *amplitude* and *topology* of the quasi-energy resonances.

The intrinsic self-similar structures of these quasi-periodic Wannier–Stark spectra are associated with incommensurate values of the ratio between the Bloch (T_o) and the driving (T) period and departs, for example, from other AC-driven Wannier–Stark spectra investigated previously [32]. The ratio T/T_o plays here the role of a scaling parameter which is experimentally easily accessible, making the observation of self-similar spectra associated with quasi-periodic Wannier–Stark quasi-energies of an atomic wavepacket rather viable. Although these phenomena could be observed in systems where Bloch oscillations have been realized, such as optically excited semiconductor superlattices [10–12,44] (see the review by Lyssenko & Leo [45]) and coupled optical waveguides [46,47], quantum gases in optical lattices realize practicable artificial solids with a higher degree of control and manipulation. They have, in fact, become a powerful

[12]More precisely, the quasi-energy components' amplitudes are displayed here through a grey-scale colour map denoting amplitudes ranging from 0 (white) to 0.20 (black) in units of $Wa/\hbar$.

experimental platform to explore matter waves' many-body interactions [1,2], matter waves' singular dynamics including electric quantum walks [48,49], super [6] and anomalous [50] Bloch oscillations as well as light-matter waves' interactions in stationary [43,51–58] and moving [59–62] ordered atomic structures trapped in an optical lattice. Within this context, it is worth mentioning the recent work [63] on cold rubidium atoms trapped in an optical lattice and subject to external lasers that impart a circular motion to them, analogous to the motion of electrons in a strong magnetic field, with which self-similar fractal structures of the spectra (*Hofstadter bands*) are expected to be seen.[13]

Acknowledgements. It is a pleasure to acknowledge enlightening conversation on the subject with M. Inguscio and A. Alberti for valuable suggestions at the early stage of this work and the CRUI-British Council Partnership Programme on 'Atoms and nanostructures'.

Appendix A

We derive an expression for the wavepacket mean position through direct evaluation of the integral on the right-hand side of (3.5). With the insertion of (2.10) into (3.5), and with the help of (3.17), the first integral can easily be shown to yield

$$\int_{-\pi/a}^{\pi/a} \mathrm{d}k|\phi(k-\theta(t),0)|^2 E(k), \tag{A 1}$$

where the Bloch eigenstate's orthogonality has been used. Similarly, by using the Schrödinger equation (2.4) in the appropriate limit, the second integral becomes

$$-\int_{-\pi/a}^{\pi/a} \mathrm{d}k|\phi(k,t)|^2 E(k) + \mathrm{i}f(t)\int_{-\pi/a}^{\pi/a} \mathrm{d}k\phi^*(k,t)\partial_k\phi(k,t), \tag{A 2}$$

where the first term exactly cancels with (A 1). When the explicit form of the atom's wave function $\phi(k,t)$ in the quasi-momentum representation in (2.9) is used, the other integral (A 2) can further be decomposed as

$$\mathrm{i}f(t)\int_{-\pi/a}^{\pi/a} \mathrm{d}k\phi^*(k-\theta(t),0)\partial_k\phi(k-\theta(t),0) + \frac{f(t)}{\hbar}\int_{-\pi/a}^{\pi/a} \mathrm{d}k|\phi(k-\theta(t),0)|^2 \times \int_0^t \mathrm{d}t'\partial_k E(k+\theta(t')-\theta(t)). \tag{A 3}$$

Owing to the periodicity $\phi(k+2\pi/a,0)=\phi(k,0)$ (reduced Brillouin zone scheme) and the fact that $\phi(k,t=0)$ can be taken as real, the former integral can be shown to vanish while the latter just yields the position average expression in (3.6). We note that, with the choice of phase of the Bloch functions used here (see footnote 1), this corresponds to the case $\langle x(t=0)\rangle = 0$.

References

1. Bloch I. 2005 Ultracold quantum gases in optical lattices. *Nat. Phys.* **1**, 23–30. (doi:10.1038/nphys138)
2. Bloch I, Dalibard J, Nascimbène S. 2012 Quantum simulations with ultracold quantum gases. *Nat. Phys.* **8**, 267–276. (doi:10.1038/nphys2259)
3. Greiner M, Mandel O, Esslinger T, Hänsch TW, Bloch I. 2002 Quantum phase transition from a superfluid to a Mott insulator in a gas of ultracold atoms. *Nature* **415**, 39–44. (doi:10.1038/415039a)
4. Dahan MB, Peik E, Reichel J, Castin Y, Salomon C. 1996 Bloch oscillations of atoms in an optical potential. *Phys. Rev. Lett.* **76**, 4508. (doi:10.1103/PhysRevLett.76.4508)
5. Anderson BP, Kasevich MA. 1998 Macroscopic quantum interference from atomic tunnel arrays. *Science* **282**, 1686—1689. (doi:10.1126/science.282.5394.1686)

[13]Bands in this case have a shape reminiscent of a *butterfly* [37] and signatures of such shapes have been seen in artificial superlattices [64–69].

6. Haller E, Hart R, Mark MJ, Danzl JG, Reichsöllner L, Nägerl H-C. 2010 Inducing transport in a dissipation-free lattice with super Bloch oscillations. *Phys. Rev. Lett.* **104**, 200403. (doi:10.1103/PhysRevLett.104.200403)
7. Raizen M, Salomon C, Niu Q. 1997 New light on quantum transport. *Phys. Today* **50**, 30. (doi:10.1063/1.881845)
8. Esaki L, Tsu R. 1970 Superlattice and negative differential conductivity in semiconductors. *IBM J. Res. Dev.* **14**, 61–65. (doi:10.1147/rd.141.0061)
9. Buttiker M, Thomas H. 1977 Current instability and domain propagation due to Bragg scattering. *Phys. Rev. Lett.* **38**, 78–80. (doi:10.1103/PhysRevLett.38.78)
10. Feldman J *et al.* 1992 Optical investigation of Bloch oscillations in a semiconductor superlattice. *Phys. Rev. B* **46**, 7252. (doi:10.1103/PhysRevB.46.7252)
11. Leo K, Bolivar PH, Brüggemann F, Schwedler R. 1992 Observation of Bloch oscillations in a semiconductor superlattice. *Solid State Commun.* **84**, 943–946. (doi:10.1016/0038-1098(92)90798-E)
12. Waschke C, Roskos HG, Schwedler R, Leo K, Kurz H, Köhler K. 1993 Coherent submillimeter-wave emission from Bloch oscillations in a semiconductor superlattice. *Phys. Rev. Lett.* **70**, 3319. (doi:10.1103/PhysRevLett.70.3319)
13. Battesti R, Cladé P, Guellati-Khélifa S, Schwob C, Grémaud B, Nez F, Julien L, Biraben F. 2004 Bloch oscillations of ultracold atoms: a tool for a metrological determination of h/m_{Rb}. *Phys. Rev. Lett.* **92**, 253001. (doi:10.1103/PhysRevLett.92.253001)
14. Ferrari G, Poli N, Sorrentino F, Tino GM. 2006 Long-lived Bloch oscillations with bosonic Sr atoms and application to gravity measurement at the micrometer scale. *Phys. Rev. Lett.* **97**, 060402. (doi:10.1103/PhysRevLett.97.060402)
15. Gustavsson M, Haller E, Mark MJ, Danzl JG, Hart R, Daley AJ, Nägerl H-C. 2010 Interference of interacting matter waves. *New J. Phys.* **12**, 065029. (doi:10.1088/1367-2630/12/6/065029)
16. Morsch O, Müller JH, Cristiani M, Ciampini D, Arimondo E. 2001 Bloch oscillations and mean-field effects of Bose–Einstein condensates in 1D optical lattices. *Phys. Rev. Lett.* **87**, 140402. (doi:10.1103/PhysRevLett.87.140402)
17. Gustavsson M, Haller E, Mark MJ, Danzl JG, Rojas-Kopeinig G, Nägerl H-C. 2008 Control of interaction-induced dephasing of Bloch oscillations. *Phys. Rev. Lett.* **100**, 080404. (doi:10.1103/PhysRevLett.100.080404)
18. Fattori M, D'Errico C, Roati G, Zaccanti M, Jona-Lasinio M, Modugno M, Inguscio M, Modugno G. 2008 Atom interferometry with a weakly interacting Bose–Einstein condensate. *Phys. Rev. Lett.* **100**, 080405. (doi:10.1103/PhysRevLett.100.080405)
19. Roati G, de Mirandes E, Ferlaino F, Ott H, Modugno G, Inguscio M. 2004 Atom interferometry with trapped Fermi gases. *Phys. Rev. Lett.* **92**, 230402. (doi:10.1103/PhysRevLett.92.230402)
20. Fisher MC, Madison KW, Niu Q, Raizen MG. 1998 Observation of Rabi oscillations between Bloch bands in an optical potential. *Phys. Rev. A* **58**, R2648. (doi:10.1103/PhysRevA.58.R2648)
21. Wilkinson SR, Bharucha CF, Madison KW, Niu Q, Raizen MG. 1996 Observation of atomic Wannier–Stark ladders in an accelerating optical potential. *Phys. Rev. Lett.* **76**, 4512. (doi:10.1103/PhysRevLett.76.4512)
22. Sias C, Zenesini A, Lignier H, Wimberger S, Ciampini D, Morsch O, Arimondo E. 2007 Resonantly enhanced tunneling of Bose–Einstein condensates in periodic potentials. *Phys. Rev. Lett.* **98**, 120403. (doi:10.1103/PhysRevLett.98.120403)
23. Zhao XG. 1994 The suppression of a Bloch band in a driving laser field. *J. Phys. Condensed Matter* **6**, 2751. (doi:10.1088/0953-8984/6/14/013)
24. Ashcroft N, Mermin D. 1976 *Solid state physics*. Philadelphia, PA: Saunders College.
25. Glutsch S. 2004 Nonresonant and resonant Zener tunneling. *Phys. Rev. B* **69**, 235317. (doi:10.1103/PhysRevB.69.235317)
26. Grifoni M, Hänggi P. 1998 Driven quantum tunneling. *Phys. Rep.* **304**, 229–354. (doi:10.1016/S0370-1573(98)00022-2)
27. Zhao X-G, Jahnkec R, Niuc Q. 1995 Dynamic fractional Stark ladders in dc-ac fields. *Phys. Lett. A* **202**, 297–304. (doi:10.1016/0375-9601(95)00336-2)
28. Niu Q, Zhao X-G, Georgakis GA, Raizen MG. 1996 Atomic Landau-Zener tunneling and Wannier–Stark ladders in optical potentials. *Phys. Rev. Lett.* **76**, 4504. (doi:10.1103/PhysRevLett.76.4504)
29. Yan W-X, Zhao X-G, Wang H. 1998 Coherent effects induced by dc-ac fields in semiconductor superlattices: the signature of fractional Wannier–Stark ladders. *J. Phys. Condensed Matter* **10**, L11. (doi:10.1088/0953-8984/10/1/002)

30. Shirley J. 1965 Solution of the Schroedinger equation with a Hamiltonian periodic in time. *Phys. Rev.* **138**, B979. (doi:10.1103/PhysRev.138.B979)
31. Zel'dovich YaB. 1967 The quasienergy of a quantum-mechanical system subjected to a periodic action. *Sov. Phys. JETP* **24**, 1006–1008.
32. Glueck M, Kolovskya AR, Korsch HJ. 2002 Wannier–Stark resonances in optical and semiconductor superlattices. *Phys. Rep.* **366**, 103–182. (doi:10.1016/S0370-1573(02)00142-4)
33. Madison KW, Fischer MC, Raizen MG. 1999 Observation of the Wannier–Stark fan and the fractional ladder in an accelerating optical lattice. *Phys. Rev. A* **60**, R1767. (doi:10.1103/PhysRevA.60.R1767)
34. Kohn W. 1959. Analytic properties of Bloch waves and Wannier functions. *Phys. Rev.* **115**, 809. (doi:10.1103/PhysRev.115.809)
35. Arfken GB, Weber HJ. 2001 *Mathematical methods for physicists*, 5th edn. San Diego, CA: Harcourt Academic Press.
36. Barenblatt G. 1995 *Scaling, self-similarity and intermediate asymptotic*. Cambridge, UK: Cambridge University Press.
37. Hofstadter D. 1976 Energy levels and wave functions of Bloch electrons in rational and irrational magnetic fields. *Phys. Rev. B* **14**, 2239. (doi:10.1103/PhysRevB.14.2239)
38. Moore FL, Robinson JC, Bharucha C, Williams PE, Raizen MG. 1994 Observation of dynamical localization in atomic momentum transfer: a new testing ground for quantum chaos. *Phys. Rev. Lett.* **73**, 2974. (doi:10.1103/PhysRevLett.73.2974)
39. Ivanov VV, Alberti A, Schioppo M, Ferrari G, Artoni M, Chiofalo ML, Tino GM. 2008 Coherent delocalization of atomic wave packets in driven lattice potentials. *Phys. Rev. Lett.* **100**, 043602. (doi:10.1103/PhysRevLett.100.043602)
40. Alberti A, Ivanov VV, Tino GM, Ferrari G. 2009 Engineering the quantum transport of atomic wavefunctions over macroscopic distances *Nat. Phys.* **5**, 547–550. (doi:10.1038/nphys1310)
41. Artoni M, La Rocca G, Ferrari G. 2009 Self-similar scaling in the coherent dynamics of ultracold atoms. *Phys. Rev. A* **R80**, 021604. (doi:10.1103/PhysRevA.80.021604)
42. Cladé P, de Mirandes E, Cadoret M, Guellati-Khélifa S, Schwob C, Nez F, Julien L, Biraben F. 2006 Determination of the fine structure constant based on Bloch oscillations of ultracold atoms in a vertical optical lattice. *Phys. Rev. Lett.* **96**, 033001. (doi:10.1103/PhysRevLett.96.033001)
43. Lin Y-W, Liao W-T, Peters T, Chou H-C, Wang J-S, Cho H-W, Kuan P-C, Yu IA. 2009 Stationary light pulses in cold atomic media and without Bragg gratings. *Phys. Rev. Lett.* **102**, 213601. (doi:10.1103/PhysRevLett.102.213601)
44. Flayac H, Solnyshkov DD, Malpuech G. 2011 Bloch oscillations of exciton-polaritons and photons for the generation of an alternating terahertz spin signal. *Phys. Rev.* **B84**, 125314. (doi:10.1103/PhysRevB.84.125314)
45. Lyssenko V, Leo K. 2011 Bloch oscillations and ultrafast coherent optical phenomena. In *Comprehensive semiconductor science and technology* (eds P Bhattacharya, R Fornari, H Kamimura), vol. 2, p. 343. Amsterdam, The Netherlands: Elsevier.
46. Sapienza R, Costantino P, Wiersma D, Ghulinyan M, Oton CJ, Pavesi L. 2003 Optical analogue of electronic Bloch oscillations. *Phys. Rev. Lett.* **91**, 263902. (doi:10.1103/PhysRevLett.91.263902)
47. Morandotti R, Peschel U, Aitchison JS, Eisenberg HS, Silberberg Y. 1999 Experimental observation of linear and nonlinear optical Bloch oscillations. *Phys. Rev. Lett.* **83**, 4756. (doi:10.1103/PhysRevLett.83.4756)
48. Genske M, Alt W, Steffen A, Werner AH, Werner RF, Meschede D, Alberti A. 2013 Electric quantum walks with individual atoms. *Phys. Rev. Lett.* **110**, 190601. (doi:10.1103/PhysRevLett.110.190601)
49. Cedzich C, Rybár T, Werner AH, Alberti A, Genske M, Werner RF. 2013 Propagation of quantum walks in electric fields. *Phys. Rev. Lett.* **111**, 160601. (doi:10.1103/PhysRevLett.111.160601)
50. Pettini G, Modugno M. 2011 Anomalous Bloch oscillations in one-dimensional parity-breaking periodic potentials. *Phys. Rev. A* **83**, 013619. (doi:10.1103/PhysRevA.83.013619)
51. André A, Lukin MD. 2002 Manipulating light pulses via dynamically controlled photonic band-gap. *Phys. Rev. Lett.* **89**, 143602. (doi:10.1103/PhysRevLett.89.143602)
52. Wu JH, Artoni M, La Rocca GC. 2008 Controlling the photonic band gap structure of optically driven cold atoms. *J. Opt. Soc. Am. B* **25**, 1840–1849. (doi:10.1364/JOSAB.25.001840)

53. Schilke A, Zimmermann C, Courteille PW, Guerin W. 2011 Photonic band gaps in one-dimensionally ordered cold atomic vapors. *Phys. Rev. Lett.* **106**, 223903. (doi:10.1103/PhysRevLett.106.223903)
54. Yang H, Yang L, Wang X-C, Cui C-L, Zhang Y, Wu J-H. 2013 Dynamically controlled two-color photonic band gaps via balanced four-wave mixing in one-dimensional cold atomic lattices. *Phys. Rev. A* **88**, 063832. (doi:10.1103/PhysRevA.88.063832)
55. Wu JH, Artoni M, La Rocca GC. 2010 Stationary light pulses in cold thermal atomic clouds. *Phys. Rev. A* **82**, 013807. (doi:10.1103/PhysRevA.82.013807)
56. Wu JH, Artoni M, La Rocca GC. 2010 Decay of stationary light pulses in ultracold atoms. *Phys. Rev. A* **81**, 033822. (doi:10.1103/PhysRevA.81.033822)
57. Schilke A, Zimmermann C, Courteille PW, Guerin W. 2012 Optical parametric oscillation with distributed feedback in cold atoms. *Nat. Photonics* **6**, 101–104. (doi:10.1038/nphoton.2011.320)
58. Wu JH, Artoni M, La Rocca GC. 2013 Two-color lasing in cold atoms. *Phys. Rev. A* **88**, 043823. (doi:10.1103/PhysRevA.88.043823)
59. Horsley SAR, Artoni M, La Rocca GC. 2011 Radiation damping in atomic photonic crystals. *Phys. Rev. Lett.* **107**, 043602. (doi:10.1103/PhysRevLett.107.043602)
60. Wu JH, Horsley SAR, Artoni M, La Rocca GC. 2013 Radiation damping optical enhancement in cold atoms. *Light: Sci. Appl.* **2**, e54. (doi:10.1038/lsa.2013.10)
61. Wang DW, Wang D-W, Zhou H-T, Guo M-J, Zhang J-X, Evers J, Zhu S-Y. 2013 Optical diode made from a moving photonic crystal. *Phys. Rev. Lett.* **110**, 093901. (doi:10.1103/PhysRevLett.110.093901)
62. Horsley SAR, Wu JH, Artoni M, La Rocca GC. 2013 Optical nonreciprocity of cold atom Bragg mirrors in motion. *Phys. Rev. Lett.* **110**, 223602. (doi:10.1103/PhysRevLett.110.223602)
63. Cheng C, Mueller EJ. 2013 Looking for Hofstadters butterfly in cold atoms. *Physics* **6**, 118. (doi:10.1103/Physics.6.118)
64. Jaksch D, Zoller P. 2003 Creation of effective magnetic fields in optical lattices: the Hofstadter butterfly for cold neutral atoms. *New. J. Phys.* **5**, 56. (doi:10.1088/1367-2630/5/1/356)
65. Geisler MC, Smet JH, Umansky V, von Klitzing K, Naundorf B, Ketzmerick R, Schweizer H. 2004 Detection of a Landau band-coupling-induced rearrangement of the Hofstadter butterfly. *Phys. Rev. Lett.* **92**, 256801. (doi:10.1103/PhysRevLett.92.256801)
66. Melinte S *et al.* 2004 Laterally modulated 2D electron system in the extreme quantum limit. *Phys. Rev. Lett.* **92**, 036802. (doi:10.1103/PhysRevLett.92.036802)
67. Feil T, Výborný K, Smrcka L, Gerl C, Wegscheider W. 2007 Vanishing cyclotron gaps in a two-dimensional electron system with a strong short-period modulation. *Phys. Rev. B* **75**, 075303. (doi:10.1103/PhysRevB.75.075303)
68. Dean CR *et al.* 2013 Hofstadter's butterfly and the fractal quantum hall effect in moiré superlattices. *Nature* **497**, 598–602. (doi:10.1038/nature12186)
69. Ponomarenko LA *et al.* 2013 Cloning of Dirac fermions in graphene superlattices. *Nature* **497**, 594–597. (doi:10.1038/nature12187)